Optimal Design for Flow Uniformity in Microchannel Reactors

J. M. Commenge, L. Falk, J. P. Corriou, and M. Matlosz
Laboratoire des Sciences du Génie Chimique, CNRS–INPL, Groupe ENSIC - Nancy, F-54001 Nancy, France

Velocity and residence time distributions play a crucial role in the performance of microreactors for chemical synthesis. The specific features of fluid flow through multiplate microchannel reactors are examined by an approximate pressure drop model whose validity is confirmed through comparison with more detailed finite-volume calculations. The model results allow for determination of the influence of the geometrical characteristics of the microchannel structures on the flow distributions and are used to optimize the reactor design for maximum flow uniformity.

Introduction

Recent advances in microfabrication technology offer the possibility of low cost replication of microchannel structures for industrial-scale production of fine chemicals. These reactors present advantages over macroscopic reactors, particularly with regard to heat management (Hsing et al., 2000), by facilitating isothermal operation or enabling the coupling of endothermic and exothermic reactions (Gavriilidis et al., 1998; Peterson, 1999). The use of microstructured reactors as tools for process development not only facilitates optimization of existing processes, but can reduce the lag-time between laboratory development and industrial production (Wörz et al., 2001).

In addition, the small characteristic dimensions of microchannel reactors can provide safe operation with highly reactive or hazardous products (Vlachos, 1998; Hagendorf et al., 1998), and these characteristics, combined with precise heat management, suggest new and original design concepts capable of reducing the number of reactive steps in long synthesis processes (Löwe et al., 1998). Such improvements should improve selectivity, and reduce energy consumption, separation steps, and production cost.

Due to their small dimensions, microreactors can present rapid response times that should be an advantage not only for process control, but also for certain heterogeneous catalytic reactions. Applying periodic reactant feed concentration, for example, has been shown to lead to a large increase in conversion or even selectivity for certain reactions when compared to steady-state operation (Thullie and Renken, 1993), and new microreactor properties are likely to make the required feed frequencies possible.

The use of microreactors for industrial-scale production of chemicals requires a large number of reactors in parallel, since each reactor provides only a small volume dedicated to reaction. Unfortunately, process design by this "numbering-up" approach is not exempt from some of the same difficulties encountered in traditional scale-up. In particular, the parallel process structures may exhibit poor uniformity in the fluid distribution between microchannels, which is generally undesirable and can limit severely the inherent advantages of microchannel reactors described above (Walter et al., 1999; Wiessmeier, 1997). Equal fluid velocities in the microchannels indeed are a necessary condition so as to have equal mass-transfer coefficients, heat-transfer coefficients, and space times. It is important, therefore, to design reactor geometries enabling narrow velocity distributions between channels.

The objective of the present study is to analyze the influence of the geometrical dimensions of the reactor microstructure on the velocity distribution between channels. For this purpose, an approximate model is developed, based on a simplified description of the reactor as a network of equivalent rectangular ducts. Results calculated with the approximate model are then compared to more detailed finite-volume calculations to validate the approach. Following validation, the approximate model is used to optimize the reactor geometry in order to eliminate the velocity variations responsible for difficulties in the design of production-scale devices.

Correspondence concerning this article should be addressed to M. Matlosz.

Microreactor Geometry

Choice of the microreactor geometry

In order to be used for industrial-scale production of chemicals, microreactors need to satisfy a certain number of constraints regarding materials and cost. Indeed, the material that constitutes the reactor must be adapted both chemically and mechanically to the required operating conditions, to avoid problems such as corrosion, clogging, or bending. The large number of reactors required for industrial production necessitates low manufacturing cost of each elementary unit, even if development and process scaling costs will be decreased due to duplication (Benson and Ponton, 1993). The microreactor should also enable coupling of chemical reaction and heat exchange in the unit volume. Modular geometries enabling a change in the number of channels without requiring substantial investment appear particularly promising, provided that uniform velocity distributions can be attained.

A number of different multichannel reactor geometries have been investigated and, among these, two main reactor concepts satisfy most of the above criteria. These geometries are:

- the monolith geometry, in which the inlet stream is simply distributed between all the channels of the unit through a large distribution chamber (Hönicke and Wiessmeier, 1996; Hagendorf et al., 1998; Wiessmeier and Hönicke, 1998; Bier et al., 1993; Wiessmeier et al., 1997).

- the multiplate reactor geometry, in which the inlet stream is first divided into substreams between microstructured plates and each substream then distributed between the channels of the plate (Richter et al., 1997; Ehrfeld et al., 1997; Tonkovich et al., 1998).

The monolith geometry can exhibit detrimental velocity differences between the channels, due to the formation of stationary vortices in the distribution chamber (Walter et al., 1999; Wiessmeier, 1997). In contrast to the monolith geometry, the narrower volumes in the multiplate geometry are likely to prevent the formation of undesired vortices, and CFD calculation (Commenge, 2001) has shown that this is indeed the case for most situations of practical interest. For this reason, the multiplate reactor geometry appears more attractive and has been chosen for this study.

Description of the microreactor studied

The microreactor studied in this work consists of a stack of microstructured plates (Ehrfeld et al., 1997), as shown in Figure 1 (lefthand side). The parallel channels and distribution chambers for each plate are etched into flat metallic sheets and holes are drilled from side to side into each of the four corners of the sheets to enable fluid flow perpendicularly through the stack. The flow trajectory through one plate in the stack is presented in Figure 1 (righthand side). Only one fluid substream is drawn for readability.

By placing the inlet and outlet tubes at lateral positions in the corners of the plate, as presented in Figure 1 (lefthand side), an alternating stack of symmetric plates can be assembled to allow two distinct fluid veins to flow through the reactor, with one vein dedicated to the reaction fluid and the other to the heat exchange fluid. By placing the tube openings in the corners, cocurrent or countercurrent flow can be achieved, a configuration that is not possible with central tube positions.

Calculation of the Velocity Distribution

Characteristic dimensions of the microstructured plates

The calculations presented in this work consider the fluid to be a continuous medium. For this approximation to be valid, the minimum characteristic dimension of the channels $d_{\min}$ must be significantly larger than the molecular mean free path (λ) of the process fluid. The Knudsen number, defined as the ratio $Kn = \lambda/d_{\min}$, indicates the degree of flow rarefaction. For low Knudsen numbers ($Kn \leq 0.01$), the fluid can still be considered as a continuum and Navier-Stokes equations are applicable, whereas for higher Knudsen numbers, rarefaction effects such as "slip-flow" on the walls appear, that must be taken into account (Harley et al., 1995; Piekos and Breuer, 1996).

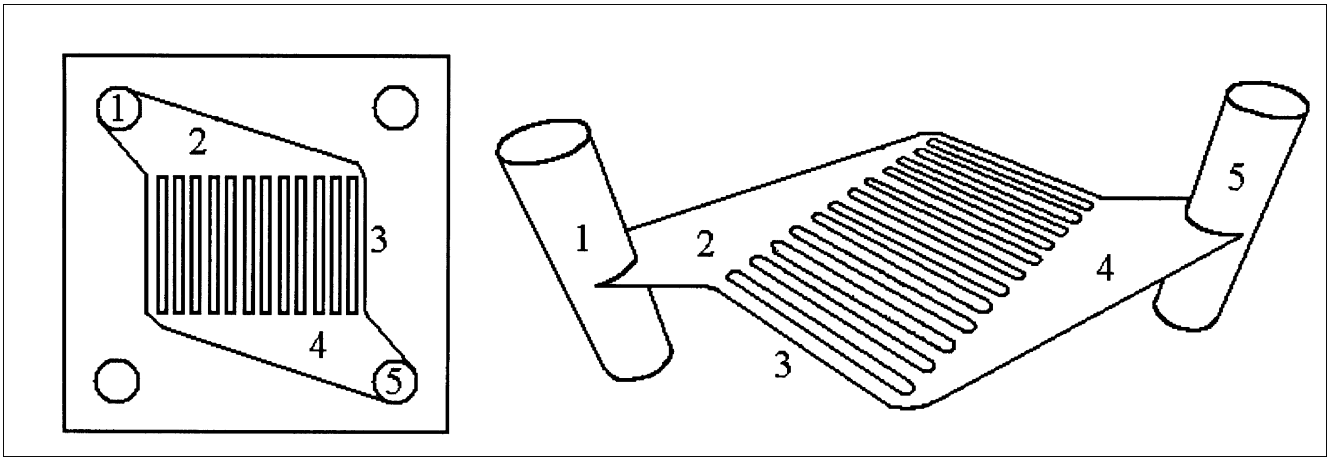

Figure 1. Microstructured plate with (1) inlet tube, (2) inlet chamber, (3) channels, (4) outlet chamber and (5) outlet tube.

From the kinetic theory of gases, the mean free path λ of a gas is directly proportional to the absolute temperature T and inversely proportional to the pressure P according to the relation (Villermaux, 1993)

$$\lambda = \frac{RT}{\pi\sqrt{2}\,PA\sigma^2} \tag{1}$$

For nitrogen, at a maximum operating temperature of 600 K and a minimum operating pressure of 1 bar, the longest mean free path reached is equal to 0.14 μm. For continuum mechanics to be valid ($Kn \leq 0.01$), the minimal characteristic channel dimension must be larger than 14 μm, which is the case for applications considered in this and many other studies (Gavriilidis et al., 1998; Hönicke and Wiessmeier, 1996; Walter et al., 1999).

In addition, this study is most particularly concerned with chemical reactions occurring in the gas phase at relatively low flow rates, for which the hydrodynamic flow regime can be considered to be laminar. For laminar duct flow in the microchannels to be valid, Reynolds numbers should be lower than 2,000, for a Reynolds number defined as

$$Re = \frac{\rho_{\text{gas}} u_{\text{gas}} D_{H_{duct}}}{\mu_{\text{gas}}} \tag{2}$$

with the hydraulic diameter of a duct with a given cross section defined as

$$D_{H_{duct}} = \frac{4S}{P_w} \tag{3}$$

For nitrogen, at 600 K and 1 bar, a Reynolds number lower than 2,000 implies $U_{\text{gas}} D_{H_{\text{duct}}}$ less than 0.01. The maximum values of the product $U_{\text{gas}} D_{H_{\text{duct}}}$ for the plates studied in this work are found in the inlet and outlet chambers where the hydraulic diameter is maximum and the cross-sectional area is minimum. In practice, velocities are lower than 10 m/s and hydraulic diameters are lower than $D_H = 500$ μm. Under these conditions, Reynolds numbers in the chambers are much lower than 2,000 and the flow regime is effectively laminar at all points on the plate.

The flow is assumed steady with no entrance effects. Neglecting entrance effects in a channel is valid for entrance lengths $L_{\text{entry}} \simeq 0.05 Re D_H$ (Midoux, 1993) significantly smaller than the channel length L_c. For a hydraulic channel diameter $D_H = 500$ μm, with nitrogen under atmospheric conditions flowing with a velocity 10 m/s, the Reynolds number in the channel is 100, which implies that the entrance length is 5 dia. long. This entrance length remains short compared to the channel length in most cases of interest. In practice, Reynolds numbers in the channels are frequently much lower, and entrance effects can often be neglected completely.

Finally, the gas is considered as incompressible. This assumption should not cause great deviations since fluid velocities U in the channels remain low, on the order of 10 m/s. The density variation of a gas can be linked to the Mach number $\boldsymbol{M}$ as (Candel, 1990)

$$\frac{\Delta\rho}{\rho} \sim \boldsymbol{M}^2 \text{ with } \boldsymbol{M} = \frac{U}{c} \tag{4}$$

For nitrogen at 600 K and 1 bar, the speed of sound c is 290 m/s leading to Mach numbers typically lower than 0.035, and incompressible flow is valid.

Detailed modeling of the reactor

Microreactor geometries can contain several hundreds to thousands of channels. For heterogeneous catalytic reactions, it is important to have equal space times in each channel of the reactor, if the catalyst coating is restricted to channels, or, in each plate, if the catalyst is also spread over the inlet and outlet chambers. Thus, it is necessary to calculate the fluid velocity over the entire reactor for proper design.

Calculation of the fluid velocity distribution over the entire reactor is possible with existing computational fluid dynamics (CFD) packages and, in the present case, the software code Fluent based on the finite-volume method (Patankar, 1980) has been used. Restricting the domain of this study to steady-state incompressible hydrodynamics and isothermal conditions, the equations to be solved in the three-dimensional (3-D) fluid domain are: the continuity equation

$$\nabla\cdot\vec{u} = 0 \tag{5}$$

and Navier-Stokes equation

$$\vec{u}\cdot\nabla\vec{u} = -\nabla P + \mu\nabla^2\vec{u} \tag{6}$$

To solve these equations, the boundary conditions assume no slip on the walls and a uniform velocity at the entrance of the inlet tube. The continuity and Navier-Stokes equations are solved for a laminar regime with negligible gravity.

Approximate model

Although possible as indicated above, complete simulation of complex reactor geometries requires nevertheless large computer resources. In the case of a reactor with a thousand channels, the calculation requires as many elementary geometric volumes as existing channels and each volume must contain a certain number of nodes. A single simulation will therefore require significant calculation time and computer memory. Furthermore, for each geometry, the simulation must be performed with varying mesh grids in order to test the influence of meshing on the computed results.

Since the present study concerns the influence of geometric parameters on the velocity distribution in the reactor, a large number of different geometries must be calculated. For engineering practice and optimization, therefore, an approximate distribution model that allows rapid calculation of the velocity distribution as a function of various geometric parameters can be a useful complement to more exact CFD calculations, and the development of such an approximate model is the primary objective of the present work. CFD calculations on selected test geometries are then used to validate the approach.

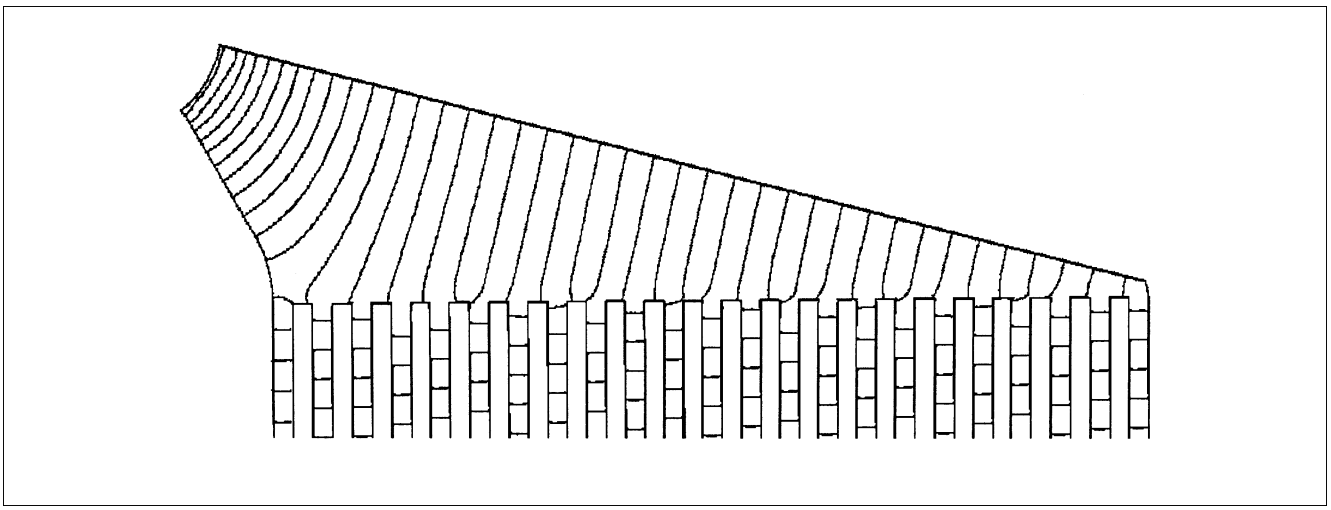

Figure 2. Finite-volume calculations of the pressure field in the inlet chamber of a plate with 23 channels.

A simple approach for studying the flow distribution in parallel structures involves calculation of the pressure variation in the distribution system and such an approach has been proposed by Bassiouny and Martin (1984) for plate heat exchangers. In some cases, the entire structure can be considered as a resistive network of ducts, where the resistances are due to flow friction (Boersma and Sammes, 1997), and a similar approach will be used for the development of the approximate model presented in this article.

To calculate the velocity distribution in the reactor, the fluid stream is divided into five zones: (1) the inlet tube, (2) the inlet chamber, (3) the channels, (4) the outlet chamber, and, (5) the outlet tube (Figure 1). With this distinction, the fluid distribution in a multiplate microchannel reactor is composed of two overlapping systems: the distribution between the channels of a given plate and the distribution from one plate to another in the multiplate stack. In this work, the approximate model for the fluid distribution between the

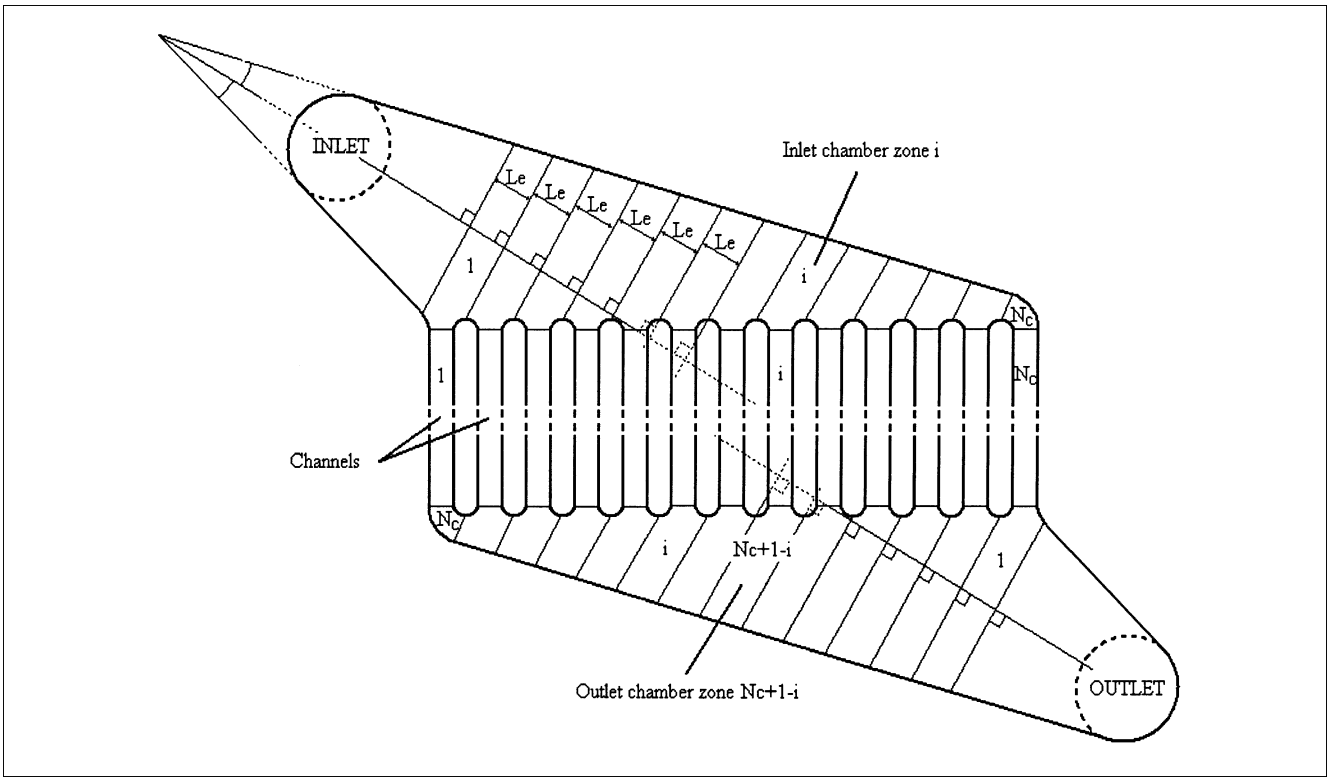

Figure 3. Description of chamber zones with corresponding channels ranging from 1 to N_c.

channels of an individual plate will be developed and detailed. A similar model can be used to describe the distribution from plate to plate and details of that approach can be found in Commenge (2001).

The absence of recirculation loops in the plate chambers has been demonstrated numerically (Commenge, 2001) and the absence of recirculation leads to a particularly simple pressure field that can be modeled easily with an approximate approach. To illustrate this point, Figure 2 presents the pressure field calculated with the finite-volume method in the inlet chamber of a plate with 23 channels. The regularity of the pressure contours illustrates the absence of recirculation, and the calculated pressure field suggests strongly that the inlet and outlet chambers can be divided into simple zones as presented in Figure 4, where the boundaries are very close to constant pressure contours. The partitioning of the inlet and outlet chambers into simple zones has been used, therefore, to construct a simplified geometry for approximate calculation.

Simplified Plate Geometry. For a plate with N_c channels, the chambers are divided into N_c zones as indicated in Figure 3. Each zone is oriented perpendicularly to a bisecting line whose origin is situated in the inlet or outlet tube associated with the corresponding chamber. The zones are equally spaced along the chamber geometry, each with an identical zone length L_e. Since the position of each zone varies along the chamber geometry, the width W_i of each zone i varies depending on its position. For all geometries studied in this work, the inlet and outlet chambers are symmetrical, leading to an identical zone construction for both chambers of a given plate.

Once the widths W_i of these N_c zones are known, the approximate model is constructed according to the principle presented in Figure 4. Each zone-channel pair is considered as a portion of a duct with a rectangular cross section along which the pressure drop can be calculated easily with standard hydraulic formulas. The resulting simplified geometry corresponds to a resistive network of ducts of uniform thickness, but with lengths and widths that vary as a function of the position of each duct in the structure.

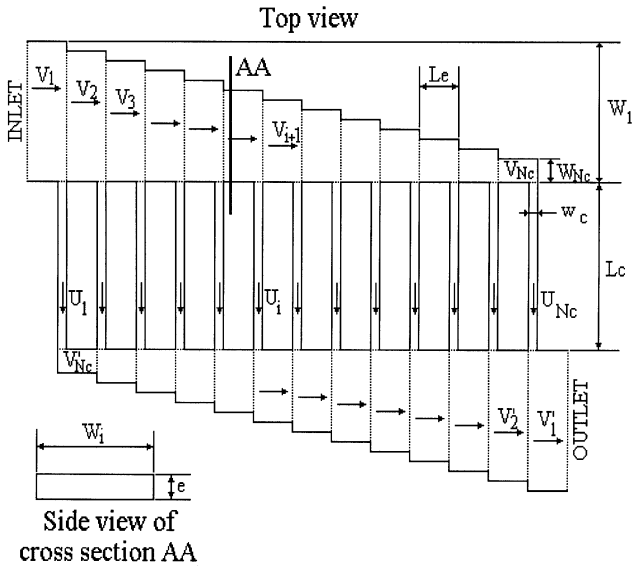

Figure 4. Channels of a plate with the different parameters and variables involved in the approximate model for velocity distribution.

Pressure Drop Through Rectangular Ducts. The linear pressure drop due to friction through a rectangular duct in laminar creeping flow, with a length L, a width w, and a thickness e, is equal to (Midoux, 1993)

$$\Delta P_f = 32\lambda_{nc}\frac{\mu L u_m}{D_H^2} \tag{7}$$

where the hydraulic diameter is defined as

$$D_H = \frac{2we}{w+e} \tag{8}$$

and the noncircularity coefficient of the duct λ_{nc} is a function of the ratio of duct thickness to duct width e/w. The complete set of equations is presented in Appendix A.

The solutions to the resulting set of equations yield the velocities in each duct of the network and in particular in the channels. The dimensionless velocity distribution (normalized with respect to the average velocity U_m through the channels) depends only on the number of channels N_c and N_c+2 dimensionless geometric ratios

$$W_i^+ = \frac{W_i}{e}, \quad L^+ = \frac{L_c}{L_e} \quad \text{and} \quad W_c^+ = \frac{W_c}{e} \tag{9}$$

where W_i^+ is the ratio of chamber width to thickness at the entrance to the i^{th} channel, L^+ is the ratio of channel length to chamber zone length, and W_c^+ is the ratio of channel width to thickness. The geometric parameters are presented in Figure 4.

The dimensionless velocity distribution between channels of a single plate does not depend on the flow rate in this simplified approach since the pressure drop considered here is only due to friction to the walls, resulting in a linear dependence of pressure drop on inlet plate velocity. If additional pressure drop contributions due to flow singularities, such as the change in duct cross section or chamber-channel intersections, are considered, the pressure-drop dependence becomes nonlinear and the distribution will depend on flow rate. These additional nonlinear effects are of secondary importance, however, and have been neglected in the approximate model.

Results

Comparison of the approximate model to finite-volume calculations

To compare calculated results obtained with the finite-volume method to those obtained with the approximate model, three standard geometries (Table 1) have been examined. The chamber geometries are not presented in detail since a complete description would require specification of all the chamber widths. Nevertheless, the three geometries are similar to the chamber geometry presented in Figure 3,

Table 1. Geometric Parameters of the Studied Plates

Number of Channels per Plate	13	23	34
Channel width (μm)	500	500	300
Channel thickness (μm)	100	500	300
Channel length (mm)	8	20	20
L^+	9.5	25.5	38.6
W_c^+	5	1	1
W_1^+	45	11	18

with regularly decreasing widths. The dimensionless widths of the first zone for each of the three cases are reported in Table 1.

The flow in each of the above geometries is simulated both by the approximate model and by finite-volume calculations (Fluent). Figure 5 presents the normalized velocity distribution between the channels of the plate with 23 channels, calculated with the approximate model (left) and the finite-volume method (right). Velocities are normalized with respect to the mean velocity through the channels. The mean velocities vary by less than 1% between the two methods in all cases. For structured mesh grids, an increase from 20,000 to 50,000 nodes results in no significant variation in the calculated distribution.

The calculated velocity distributions appear to be symmetric. This result is expected since the plate geometry is center-symmetric, although it cannot be proven directly from the equation set of the approximate model. In fact, whereas the velocity distribution is always found to be exactly symmetric for the approximate model, the finite-volume results show slight asymmetry, increasing with increasing inlet velocity.

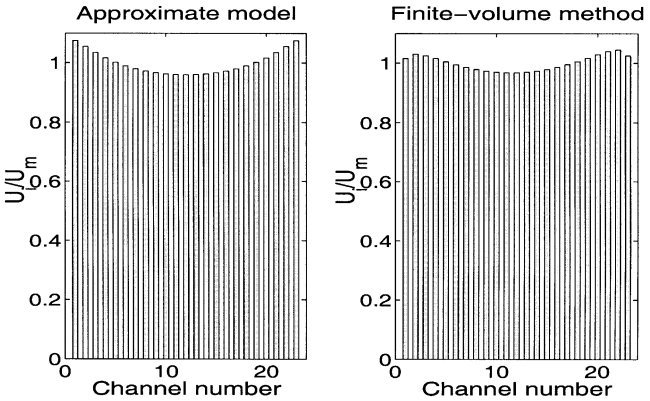

Figure 5. Normalized velocity distribution in the 23-channel plate calculated with the approximate model (left) and the finite-volume method (right).

For the microreactor geometry calculated in Figure 5, a convex velocity distribution is found with the lowest velocity in the middle channel and the highest velocitites in the channels along the edge. The shape of the distribution depends strongly on the geometry of the inlet and outlet chambers. Figure 6 shows the variation of distribution shape as a function of the width of the last inlet zone for a plate with linear chambers and 20 channels. Whereas a minimum velocity appears in the middle channel for $W_{20}^+ = 10$, a maximum velocity is calculated for $W_{20}^+ = 0.5$. This shape inversion between concave and convex distributions suggests the existence of an in-

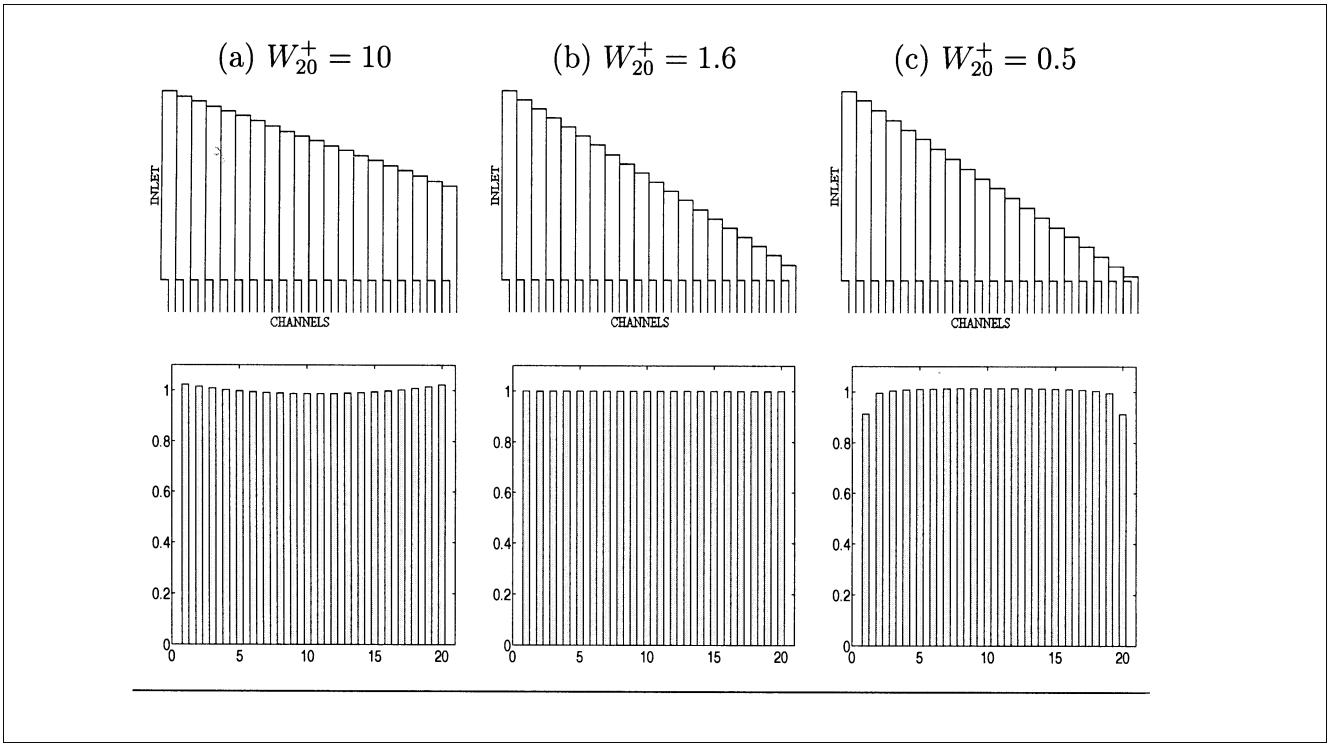

Figure 6. Normalized velocity distributions calculated using the approximate model for plates with linear chambers, 20 channels, $L^+ = 50$, $W_c^+ = 1$ and various values of W_{20}^+.

Table 2. Maximum Velocity Difference for the Reported Geometries

	Maximum Velocity Difference $\Delta U_{\%}$	
Number of Channels	Approximate Model	Finite-Volume Method
13	13.9%	10.5%
23	11.4%	7.6%
34	10.9%	7.9%

termediate geometry yielding a practically uniform distribution between the channels, and this is indeed the case for $W_{20}^{+} = 1.6$.

In order to compare the quality of velocity distributions for different geometries, a normalized maximum velocity difference, $\Delta U_{\%}$ is used as defined below

$$\Delta U_{\%} = 100. \frac{\max(U_i) - \min(U_i)}{\text{mean}(U_i)} \tag{10}$$

Table 2 presents the maximum velocity differences calculated by both methods for the geometries described in Table 1. An important feature of the equation set for the approximate model is the linearity between the pressure drop and the velocity due to the laminar flow through ducts. As a result, the normalized velocity distributions determined by the approximate model are independent of inlet velocity. Results obtained with the finite-volume method confirm this characteristic and exhibit only a slight influence of inlet velocity on the velocity distribution. Indeed, an increase of less than 1% in the maximum velocity difference is observed for a tenfold increase in Reynolds number.

The main difference observed between the velocity distributions calculated by the two methods can be seen in Figure 5 and concerns velocities in the channels near the edges. The velocities in the edge channels are lower than in neighboring channels, and this drop in the edge regions reduces the maximum velocity difference when compared to the approximate results (Table 2). A reason for this effect may be the influence of the sidewalls of the inlet and outlet chambers (Shah and London, 1978) that is not taken into account in the approximate model.

Apart from the edge effects, the comparison between the approximate model and the finite-volume method indicates good agreement for the geometries studied in all cases.

Influence of geometric parameters

For the approximate model, based on isothermal incompressible creeping flow in rectangular ducts, only geometric parameters appear in the equation system governing the fluid distribution between the channels of a microstructured plate. These geometric parameters are the N_c dimensionless chamber-zone widths W_i^{+}, the ratio L^{+} of channel length to chamber zone length, the ratio W_c^{+} of channel width to fluid vein thickness, and the number of channels N_c. The total number of parameters is therefore $N_c + 3$. A few qualitative features of the dependence of the normalized maximum velocity difference $\Delta U_{\%}$ on channel length and channel width are presented in the next sections.

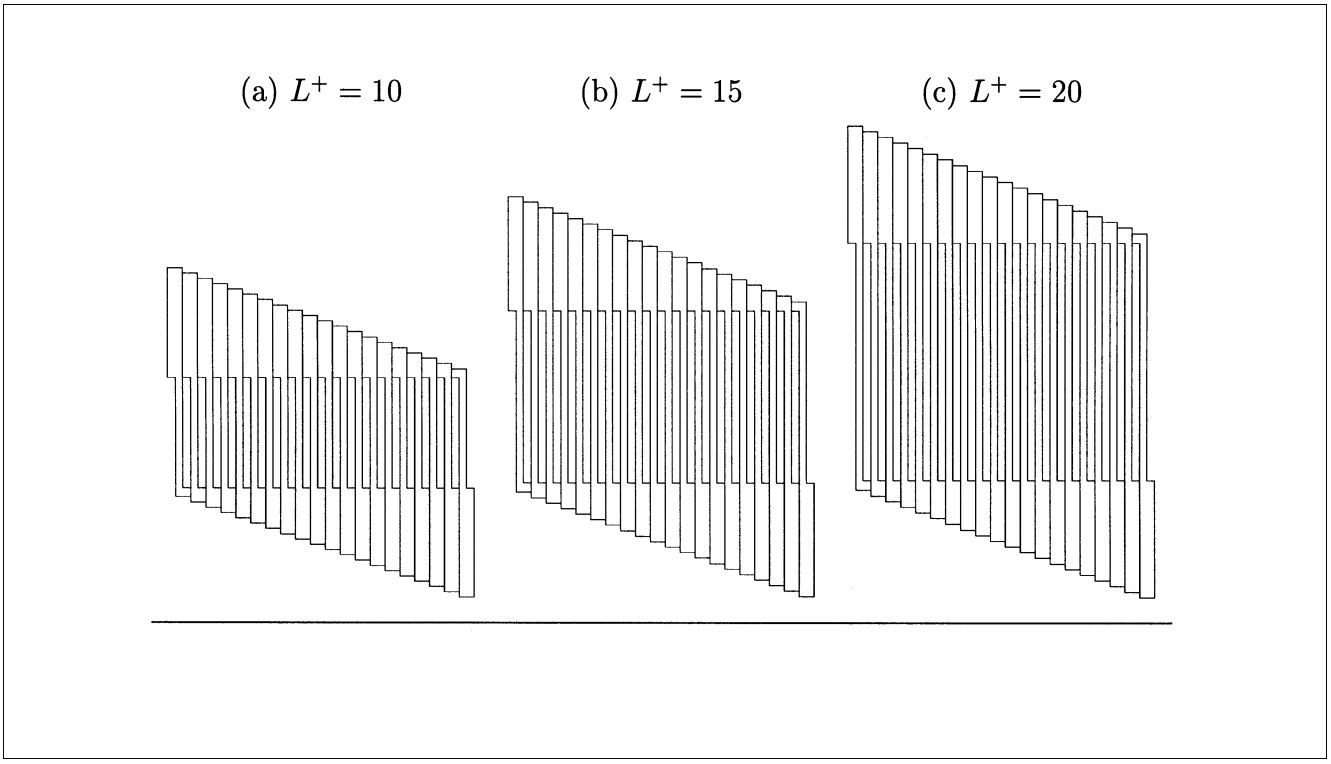

Figure 7. Influence of L^{+} on the plate geometry for fixed channel number N_c, channel width W_c, channel thickness e, zone length L_e and chamber geometry.

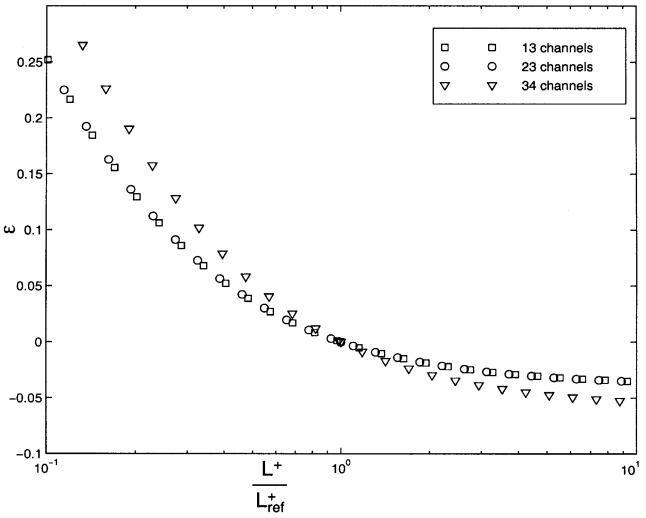

Figure 8. Correction factor ϵ (Eq. 11) as a function of the ratio L^+/L^+_{ref} for $L^+_{ref}=50$. Results are presented for the three plate geometries presented in Table 1.

Influence of Dimensionless Channel Length L^+. For a given set of parameters W_i^+, W_c^+ and N_c, the maximum velocity difference $\Delta U_{\%}$ is found to be roughly inversely proportional to dimensionless channel length L^+. Figure 7 presents three plate geometries to visualize the influence of L^+. A reciprocal dependence of the maximum velocity difference with respect to L^+ is not surprising since the velocity distribution between channels is due to a pressure drop balance between the channels and the chamber zones. According to Eq. A3, the fluid velocity difference between adjacent channels depends on pressure drop through the channels and through the corresponding chamber zones. Since equal velocities in adjacent channels require equal pressure drop through the channels (higher L^+) should result in a more uniform velocity distribution.

From a reference value $\Delta U_{\%,\mathrm{ref}}$, calculated for a chosen reference length L^+_{ref}, the maximum velocity difference $\Delta U_{\%}$ for any other L^+ can be estimated approximately as follows

$$\Delta U_{\%} = \Delta U_{\%,\mathrm{ref}} \frac{L^+_{\mathrm{ref}}}{L^+}(1-\epsilon) \tag{11}$$

where ϵ should represent in general a small correction.

Figure 8 presents the variation of the correction factor ϵ for the three plate geometries of Table 1, for a reference value $L^+_{\mathrm{ref}}=50$. The figure is plotted for the plate geometries described in Table 1 for values of L^+ ranging from 5 to 500. As a consequence, the ratio L^+/L^+_{ref} ranges from 0.1 to 10. The correction factor ϵ can be seen to decrease slightly with an increase in the ratio L^+/L^+_{ref}.

Influence of Dimensionless Channel Width W_c^+. Figure 9 shows the qualitative variation of $\Delta U_{\%}$ calculated as a function of the dimensionless channel width W_c^+. A square channel corresponds to $W_c^+=1$. Thus, values of W_c^+ less than 1 correspond to narrow channels, values of W_c^+ greater than 1 to wide channels. Figure 10 presents three different channel cross sections obtained with varying dimensionless widths W_c^+. To facilitate comparison of different cases on a single graph, $\Delta U_{\%}$ is normalized with respect to its value calculated for square channels

$$\frac{\Delta U_{\%}}{\Delta U_{\%,W_c^+=1}} \tag{12}$$

The plotted values are calculated for several plate geometries. The trend is the same in all cases: the maximum velocity difference increases with increasing channel width W_c^+. Two variation domains can be seen: the ratio $\Delta U_{\%}/\Delta U_{\%,W_c^+=1}$ evolves rapidly for narrow channels whereas the influence of

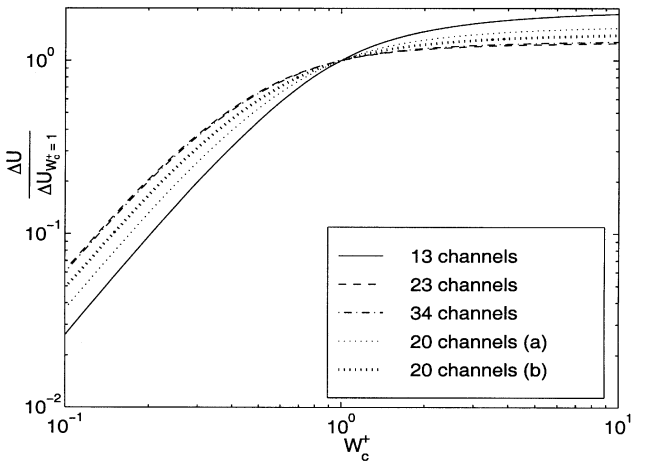

Figure 9. Normalized velocity difference $\Delta U_{\%}$ (Eq. 10) with respect to the ratio W_c^+, for the plate geometries presented in Tables 1 and 2.

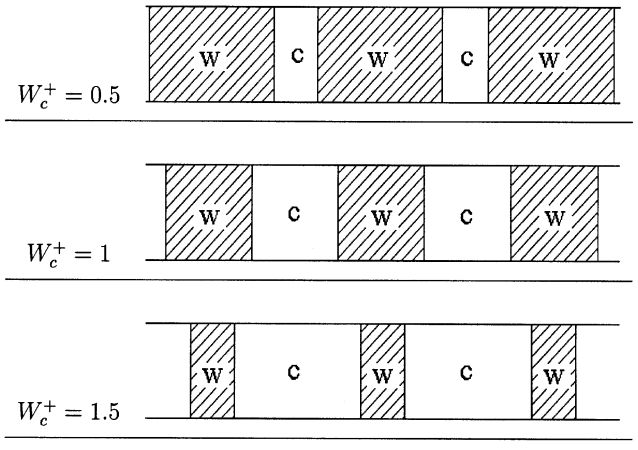

Figure 10. Influence of W_c^+ on channel cross section c, and on wall cross section W, for fixed channel number N_c, channel thickness e, dimensionless length L^+ and chamber geometry.

W_c^+ is weaker for wide channels. As for the influence of L^+ described above, the influence of W_c^+ can be explained from pressure drop considerations. Indeed, increasing W_c^+ increases the cross section for fluid flow through the channels, thereby decreasing the pressure drop through the channels compared to the pressure drop in the chambers that remains unchanged. As a result, velocity nonuniformities increase with W_c^+.

Optimization of the Chamber Geometry

Purpose

For applications of microchannel reactors for heterogeneous catalysis, chemical reaction is most often restricted to the catalyst-coated walls of the channels. Reliable scale-up of such systems requires therefore equal velocities through each of the channels in the structure. The approximate pressure-drop model will be used in the following section to obtain a velocity distribution between the channels of the reactor that is as uniform as possible. Uniformity will then be verified by finite-volume calculations on the predicted structure.

Condition on chamber geometry

The pressure drop relation for the approximate model (Eq. A3) results from the assumption that the boundaries of chamber zones are iso-pressure contours. As a result, pressure at the entrance to channel i and to inlet zone i are equal. Equal velocities in the channels i and $i+1$ imply equal pressure drops through these channels

$$\Delta P_{\text{channel } i} = \Delta P_{\text{channel } i+1} \qquad \text{for } 1 \le i \le N_c - 1 \tag{13}$$

Using Eq. A3 and the mass balances presented in Appendix B, the condition for a uniform velocity distribution between the channels implies the equality condition

$$\frac{N_c - i}{W_{i+1}^+\left(1 - 0.351\dfrac{1}{W_{i+1}^+}\right)^2} = \frac{i}{W_{N_c+1-i}^+\left(1 - 0.351\dfrac{1}{W_{N_c+1-i}^+}\right)^2} \tag{14}$$

resulting in a direct relation between the width W_{i+1}^+ of inlet zone $i+1$ and the width $W_{N_c+1-i}^+$ of outlet zone N_c+1-i.

Determination of an optimum chamber geometry yielding a uniform velocity distribution can be performed by calculating the widths W_i^+ satisfying the above condition. With no further assumptions, Eq. 14 results in $N_c/2-1$ equations relating the W_i^+ if N_c is an even number and $(N_c-1)/2$ equations if N_c is an odd number.

Choice of the optimization criterion

In order to obtain a uniform velocity distribution, the following criterion J to be minimized can be defined

$$J = \sum_{i=1}^{i=N_c} \left| 1 - \frac{U_i}{U_m} \right| \tag{15}$$

J is equal to zero if the widths W_i^+ exactly satisfy condition 14.

It should be noted, however, that Eq. 14 only relates an inlet zone to a corresponding outlet zone and does not relate the various inlet zones to each other. Consequently, an infinite number of optimum chamber geometries can be determined. Indeed, for an optimized chamber geometry, one inlet zone and its corresponding outlet zone can be modified, while keeping other zone widths constant, to find new widths that will also satisfy condition 14. Hence, it is possible to design optimized chambers with unrealistic or technically unfeasible width profiles. This point highlights the fact that a relation between adjacent zones is required so that the geometry may be regular enough to avoid recirculation or additional hydrodynamic singularities, and be simple to produce.

For this reason, a second term is added to the optimization criterion to yield the following two-term condition

$$J = \sum_{i=1}^{i=N_c} \left| 1 - \frac{U_i}{U_m} \right| + \xi \sum_{i=2}^{i=N_c} \left| 1 - \frac{W_{i,lin}}{W_i} \right| \tag{16}$$

where the width $W_{i,lin}$ is defined as

$$W_{i,lin} = W_2 + \frac{i-1}{N_c - 2}\left(W_{N_c} - W_2\right) \tag{17}$$

The second term evaluates the difference between the optimized chamber geometry and a linear chamber based on the width of the first and last zones. The width W_1 does not appear in this expression since it is not a parameter of influence in the optimization process. Furthermore, the second term in criterion 16 is weighted with a numerical factor ξ, so that both terms may have the same order of magnitude. The factor ξ is fixed at the beginning of the calculation and kept constant thereafter.

General case

The optimization process thus consists of minimizing the criterion J defined in Eq. 16 for fixed values of N_c, L^+ and W_c^+. The problem is also constrained since every variable W_i^+ ranges between a lower and an upper limit. The optimization method used to solve the problem is based on the gradient projection method and uses a limited memory BFGS matrix to approximate the Hessian of the objective function. A full description of the method can be found in Byrd et al. (1995) and Fletcher (1991).

Example of an optimized chamber

As an example, the optimization process has been applied to the plate geometry with 23 channels, whose dimensions are presented in the Table 1. The numerical parameter ξ is equal to 0.01. The optimized geometry is presented in Figure 11.

Optimized geometries yield velocity differences that are lower than a hundredth of a percent. The obtained shape is quite regular, but also complex, since a slight curvature appears along the chamber wall. As a result, such a geometry may be technically quite difficult to produce in the microfab-

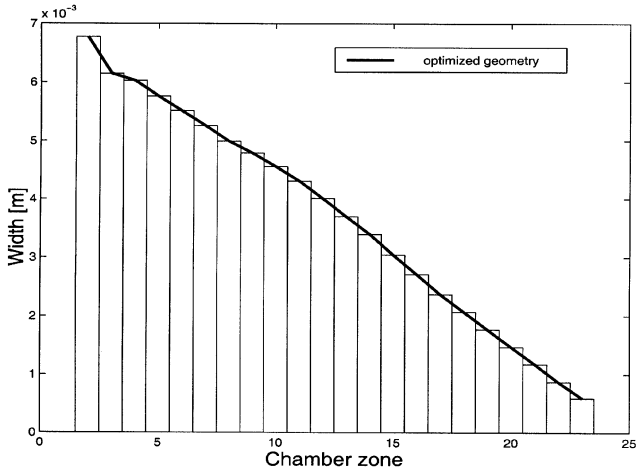

Figure 11. Optimized chamber geometry of the plate with 23 channels.

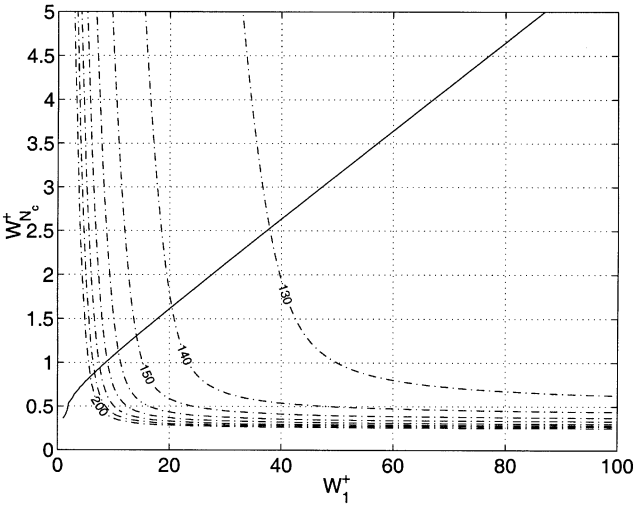

Figure 12. Values of W_1^+ and $W_{N_c}^+$ (solid line) yielding the most uniform velocity distributions for a plate with linear chambers, $L^+ = 50$, $W_c^+ = 1$, and $N_c = 20$ channels.

Values of the pressure drop parameter ranging from 130 to 200 are also shown (dashed lines).

rication process of the plate. For this reason, the following paragraphs will focus on the special case of linear chambers, whose fabrication should be easier.

Special case of a linear chamber

For a linear chamber geometry, the number of parameters is reduced to

$$L^+, W_c^+, W_1^+, W_{N_c}^+, N_c \tag{18}$$

since the widths of the chamber zones are related to each other through the relation

$$W_i^+ = W_1^+ + \frac{i-1}{N_c - 1}\left(W_{N_c}^+ - W_1^+\right) \tag{19}$$

While the study of linear chambers is important to simplify design of technically feasible microstructured reactors, this case is only an approximation of the generalized optimization process. Indeed, the constraint of a linear chamber wall is too strong to allow completely uniform velocity distributions to be obtained. Nevertheless, the differences can be reduced to less than a few percent in most cases, which is sufficient for practical application.

For the linear chambers, direct calculation has been used and an optimization procedure is not employed. For fixed values of N_c, L^+, and W_c^+, all possible linear chamber geometries can be represented as points $(W_1^+; W_{N_c}^+)$ in a 2-D parameter space. Direct calculations of velocity nonuniformity with the approximate model can be used to determine a curve in $(W_1^+; W_{N_c}^+)$ space along which nonuniformity is minimal.

To choose an acceptable geometry among the possibilities offered by the minimization curve, an additional criterion must be used. For reactor design, pressure drop through the microstructured plate is often an important consideration. The pressure drop can be calculated by following any of the N_c substreams flowing through the channel structure. The pressure drop of a substream j is

$$\Delta P_{\text{plate}} = \sum_{i=1}^{j} \Delta P_i^{\text{inlet zone}} + \Delta P_{\text{channel } j} + \sum_{i=1}^{N_c - 1 - j} \Delta P_i^{\text{outlet zone}} \tag{20}$$

Using Eqs. A2 and A1, this equation can be written in its dimensionless form as

$$\frac{\Delta P_{\text{plate}} e^3}{12\mu L_e W_c U_c} = \frac{L^+}{W_c^+\left(1 - 0.351\dfrac{1}{W_c^+}\right)^2} + \sum_{i=1}^{N_c} \frac{(N_c + 1 - i)}{W_i^+\left(1 - 0.351\dfrac{1}{W_i^+}\right)^2} + \frac{N_c}{W_1^+\left(1 - 0.351\dfrac{1}{W_1^+}\right)^2} \tag{21}$$

in terms of a dimensionless pressure drop parameter $\Delta P_{\text{plate}} e^3 / 12\mu L_e W_c U_c$.

To summarize, the approximate optimization process calculates the chamber geometry $(W_1^+; W_{N_c}^+)$ that gives the minimum velocity difference between the channels of a plate for given geometric parameters L^+, W_c^+, N_c, and dimensionless pressure drop $\Delta P_{\text{plate}} e^3 / 12\mu L_e W_c U_c$.

Optimized linear chambers

Figure 12 presents the results obtained for a plate with 20 channels and linear chambers. The solid line presents the linear chamber geometries $(W_1^+, W_{N_c}^+)$ giving the most uniform velocity distributions. The dashed lines present the geometries corresponding to dimensionless pressure drop parameters $\Delta P_{\text{limit}} e^3 / 12\mu L_e W_c U_c$ ranging from 130 to 200. For example, the optimized chamber for a pressure drop parameter

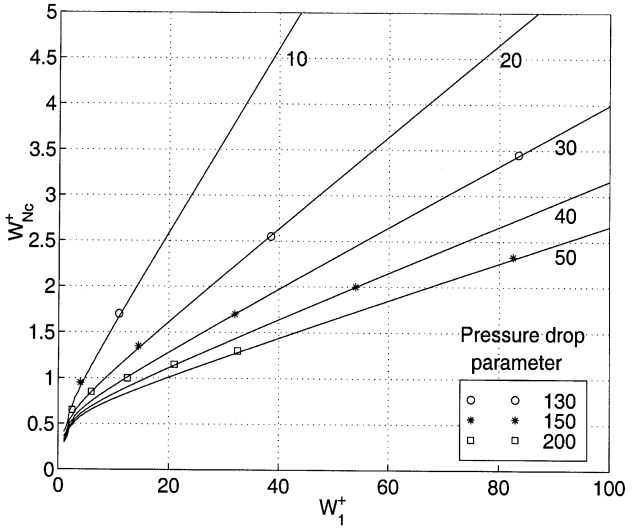

Figure 13. Values of W_1^+ and $W_{N_c}^+$ yielding the most uniform velocity distributions for plates with linear chambers, $L^+ = 50$, $W_c^+ = 1$, for numbers of channels, N_c, ranging from 10 to 50 and indicative values of the pressure drop parameter ranging from 130 to 200.

equal to 130 has its first dimensionless width W_1^+ and its last width $W_{N_c}^+$ equal to 37.5 and 2.51, respectively.

As indicated previously, this approximate optimization does not yield a perfectly uniform velocity distribution. Minimum nonuniformity increases slightly with decreasing W_1^+. Nevertheless, for W_1^+ greater than 3, nonuniformities in this case are at most 2%.

This calculation has also been performed for plates with 10, 30, 40 and 50 channels. A summary of the results is presented in Figure 13. For each case, the solid line presents the linear chamber geometries yielding the most uniform distributions between the channels. For readability, the families of lines presenting the pressure drop parameter are not shown, but a few values of this pressure drop parameter are reported on the uniform distribution curves for information.

Here again, the optimum velocity distributions are not perfectly uniform. For a plate with 50 channels, $W_c^+ = 1$ and $L^+ = 50$, for example, geometries with W_1^+ larger than 15 yield at most 1% differences, whereas, for W_1^+ greater than 10, the differences are never greater than 3%. For plates with a large number of channels, linear chamber geometries may not be sufficient for adequate flow uniformity. For such cases, the general optimization method (nonlinear chambers) can be used.

Use of the results for the design of microstructured plates

For engineering practice, the design of optimal microstructured plate geometries for a given application will generally involve several steps. A typical design sequence might resemble the following procedure:

- First, the width W_c and the thickness e of the channels are chosen depending on mass-transfer considerations between the bulk fluid and the coated wall, particularly for heterogeneously catalyzed reactions.
- The thickness of the walls between channels can be chosen based on heat exchange considerations, if required, as well as the technical capabilities of the microfabrication process and the mechanical resistance of the reactor. Wall thickness and channel width determine the chamber zone length L_e (Figure 3).
- Next, the channel length L_c and the fluid velocity U_c are chosen, depending on the space time required for reaction in the channels, as well as the maximum pressure drop through the reactor.
- The total number of channels N_c can then be calculated depending on the flow rate that must circulate through each plate.
- Once all other geometric parameters have been determined, the optimum linear chamber can be designed by using optimization results such as Figure 13 to determine the widths of the first and last zones of the chamber, as a function of the pressure drop through an individual plate.

Conclusion

Microstructured reactors are currently used as effective tools for process development, and their use for industrial-scale production of fine chemicals can be envisioned in the near future thanks to advances in microfabrication technologies. Such reactors should offer new possibilities such as enhanced heat exchange, improved process control, and inherent safety due to the specific geometrical features of their microchannel structures.

An understanding of the fluid distribution in the parallel process structures required for chemical production in microchannel systems is critical for industrial scale-up. It is therefore of interest to develop a tool to estimate quickly the quality of the distribution and the maximum velocity difference attained in the reactor.

In this work, a multiplate microchannel reactor, consisting of a stack of microstructured plates has been investigated. The study compares two approaches: an approximate pressure drop model and more detailed finite-volume calculations. The results obtained by the approximate model, based on pressure drop calculations through a resistive network of ducts, are shown to be in good agreement with those obtained with the finite-volume method. The approximate model provides rapid calculation of the fluid distribution and offers a qualitative understanding of the influence of geometric parameters and characteristic dimensions on the quality of fluid distribution among the channels of a microstructured plate.

In addition, the approximate model can be used to design plate geometries resulting in uniform velocity distributions between the channels. Finite-volume calculations confirm the validity of the optimized designs.

The approximate pressure drop model has been applied in this work to an individual microchannel plate, but a similar approach is also possible for estimations of plate-to-plate variations in flow, thereby allowing for optimization of inlet and outlet tube geometries as well.

Notation

A = Avogadro number
c = speed of sound, m/s
$d_{\min}$ = minimal characteristic dimension, m

D_H = hydraulic diameter, m
e = duct thickness, m
g = gravitational acceleration, m^2/s
Kn = Knudsen number
L = duct length, m
L_c = channel length
L_e = chamber zone length, m
L_{entry} = hydrodynamic entrance length, m
L^+ = ratio of channel length to zone length
M = Mach number
N_c = number of channels per plate
P_w = wetted perimeter, m
P = pressure, Pa
R = universal gas constant, J/mol/K
Re = Reynolds number
S = cross section, m^2
T = absolute temperature, K
u = fluid velocity, m/s
u_m = mean velocity, m/s
U_i = velocity in channel i, m/s
V_i = velocity in inlet zone i, m/s
$0V_i'$ = velocity in outlet zone i, m/s
w = duct width, m
W_c = channel width, m
$0W_c^+$ = dimensionless channel width
$0W_i$ = width of inlet and outlet zones i, m
$0W_i^+$ = dimensionless zone width

Greek letters

ΔP_f = pressure drop due to friction, Pa
$\Delta U_{\%}$ = maximum velocity difference
ϵ = correction factor
λ = molecular mean free path, m
λ_{nc} = noncircularity coefficient
μ = dynamic viscosity, Pa·s
ξ = optimization parameter
ρ = density, kg/m^3
σ = molecular diameter, m

Literature Cited

Bassiouny, M. K., and H. Martin, "Flow Distribution and Pressure Drop in Plate Heat Exchangers—I," *Chem. Eng. Sci.*, **39**, 4, 693 (1984).

Benson, R. S., and J. W. Ponton, "Process Miniaturisation—A Route to Total Environmental Acceptability?," *Trans. Inst. Chem. Eng.*, **71**, 160 (1993).

Bier, W., W. Keller, G. Linder, D. Seidel, K. Schubert, and H. Martin, "Gas to Gas Heat Transfer in Micro Heat Exchangers," *Chem. Eng. Proc.* **32**, 33 (1993).

Boersma, R. J., and N. M. Sammes, "Distribution of Gas Flow in Internally Manifolded Solid Oxide Fuel-Cell Stacks," *J. of Power Sources*, **66**, 41 (1997).

Byrd, R. H., P. Lu, J. Nocedal, and C. Zhu, "A Limited Memory Algorithm for Bound Constrained Optimization," *SIAM J. Scientific Computing*, **16**, 5, 1190 (1995).

Candel, S., *Mécanique des Fluides*, Dunod Université, Paris (1990).

Commenge, J. M., "Réacteurs Microstructurés: Hydrodynamique, Thermique, Transfert de Matière et Applications aux Procédés," PhD Thesis, INPL, Nancy, France (Oct. 2001).

Ehrfeld, W., C. Gärtner, K. Golbig, V. Hessel, R. Konrad, H. Löwe, T. Richter, and C. Schulz, "Fabrication of Components and Systems for Chemical and Biological Microreactors," *Proc. of First Int. Conf. on Microreaction Technol.*, W. Ehrfeld, Springer, Berlin/Heidelberg, Germany, 72 (1997).

Fletcher, R., *Practical Methods of Optimization*, Wiley, Chichester, U.K. (1991).

Gavriilidis, A., S. Konstantinidis, and D. Gobby, "Interaction of Endothermic and Exothermic Reactions in Microreactors," *Proc. of Second Int. Conf. on Microreaction Technol.*, New Orleans, 211 (Mar. 8–12, 1998).

Hagendorf, U., M. Janicke, F. Schüth, K. Schubert, and M. Fichtner, "A Pt/Al_2O_3 Coated Microstructured Reactor/Heat Exchanger for the Controlled H_2O/O_2-Reaction in the Explosion Regime," *Proc. of Second Int. Conf. on Microreaction Technol.*, New Orleans, 81 (Mar. 8–12, 1998).

Harley, J. C., Y. Huang, H. H. Bau, and J. N. Zemel, "Gas Flow in Micro-Channels," *J. Fluid Mech.*, **284**, 257 (1995).

Hönicke, D., and G. Wiessmeier, "Heterogeneously Catalysed Reactions in a Microreactor," *Microsystem Technol. for Chem. and Biological Microreactors, DECHEMA Monographs*, **132**, 93 (1996).

Hsing, I. M., R. Srinivasan, M. P. Harold, K. F. Jensen, and M. A. Schmidt, "Simulation of Micromachined Chemical Reactors for Heterogeneous Partial Oxidation Reactions," *Chem. Eng. Sci.*, **55**, 3 (2000).

Löwe, H., W. Ehrfeld, K. Gebauer, K. Golbig, O. Hausner, V. Haverkamp, V. Hessel, and T. Richter, "Microreactor Concepts for Heterogeneous Gas Phase Reactions," *Proc. of Second Int. Conf. on Microreaction Technol.*, New Orleans, 63 (Mar. 8–12, 1998).

Midoux, N., *Mécanique et Rhéologie des Fluides en Génie Chimique*, Lavoisier TEC & DOC, Paris (1993).

Patankar, S. V., *Numerical Heat Transfer and Fluid Flow*, Hemisphere Publishing Corporation, New York (1980).

Peterson, R. B., "Numerical Modeling of Conduction Effects in Microscale Counterflow Heat Exchangers," *Microscale Thermophys. Eng.*, **3**, 17 (1999).

Piekos, E. S., and K. S. Breuer, "Numerical Modeling of Micromechanical Devices Using the Direct Simulation Monte Carlo Method," *J. Fluid Eng.*, **118**, 464 (1996).

Richter, T., W. Ehrfeld, A. Wolf, H. P. Gruber, and O. Wörz, "Fabrication of Microreactor Components by Electro Discharge Machining," *Microreaction Technol., Proc. of First Int. Conf. on Microreaction Technol.*, 158 (1997).

Shah, R. K., and A. L. London, *Laminar Flow Forced Convection in Ducts*, Academic Press, New York (1978).

Thullie, J., and A. Renken, "Model Discrimination for Reactions with a Stop-Effect," *Chem. Eng. Sci.*, **48**, 3921 (1993).

Tonkovich, A. L. Y., J. L. Zilka, M. R. Powell, and C. J. Call, "The Catalytic Partial Oxidation of Methane in a Microchannel Chemical Reactor," *Proc. of the Second Int. Conf. on Microreaction Technol.*, New Orleans, 45 (Mar. 8–12, 1998).

Villermaux, J., *Génie de la Réaction Chimique, Conception et Fonctionnement des Réacteurs*, Lavoisier TEC & DOC, Paris (1993).

Vlachos, D. G., "Stochastic Modeling of Chemical Microreactors with Detailed Kinetics Induction Times and Ignitions of H_2 in Air," *Chem. Eng. Sci.*, **53**, 157 (1998).

Walter, S., G. Frischmann, R. Broucek, M. Bergfeld, and M. Liauw, "Fluiddynamikaspekte in Mikrostrukturreaktoren," *Chem. Ing. Tech.*, **71**, 447 (1999).

Wiessmeier, G., *Monolithische Mikrostrukturreaktoren mit Mikroströmungskanälen und regelmässigen Mesoporensystemen für selektive heterogen katalysierte Gasphasenreaktionen*, Shaker Verlag, Aachen (1997).

Wiessmeier, G., and D. Hönicke, "Strategy for the Development of Microchannel Reactors for Heterogeneously Catalyzed Reactions," *Proc. of the Second Int. Conf. on Microreaction Technol.*, New Orleans, 24 (Mar. 8–12, 1998).

Wiessmeier, G., K. Schubert, and D. Hönicke, "Monolithic Microreactors Possessing Regular Mesopore Systems for the Successful Performance of Heterogeneously Catalysed Reactions," *Microreaction Technol., Proc. of First Int. Conf. on Microreaction Technol.*, **20** (1997).

Wörz, O., K. P. Jäckel, T. Richter, and A. Wolf, "Microreactors—A New Efficient Tool for Reactor Development," *Chem. Eng. Technol.*, **24**, 138 (2001).

Appendix A: Equations for the Velocity Distribution

The noncircularity coefficient of a rectangular duct is defined as

$$\lambda_{nc} = \frac{\frac{3}{2}}{\left(\left(1-0.351\frac{e}{w}\right)\left(1+\frac{e}{w}\right)\right)^2} \quad \text{for} \quad 0 \le \frac{e}{w} \le 1 \quad \text{(A1)}$$

For the case where $e/w > 1$, λ_{nc} can be obtained by replacing e/w by w/e in Eq. A1. Consequently, the general form of Eq. 7 becomes, for all values of e/w

$$\Delta P_f = 12 \frac{\mu L u_m}{\min^2(e, w)\left(1 - 0.351 \min\left(\frac{w}{e}, \frac{e}{w}\right)\right)^2} \quad \text{(A2)}$$

To facilitate the readibility of the text, the complete set of equations is presented here for a ratio e/w less than unity.

In order to calculate the velocity distribution between the channels, one can consider two adjacent channels and the inlet and outlet zones that separate them. In this presentation, channels i and $i+1$, inlet zone $i+1$, and outlet zone N_c+1-i are considered. If the fluid flows through channel i and outlet zone N_c+1-i, its pressure drop is the same as if it had flown through inlet zone $i+1$ and channel $i+1$

$$\Delta P_{\text{channel, } i} + \Delta P_{\text{outlet zone } N_c+1-i} = \Delta P_{\text{inlet zone, } i+1} + \Delta P_{\text{channel } i+1} \quad \text{for} \quad 1 \le i \le N_c - 1 \quad \text{(A3)}$$

Including Eq. A2 and simplifying yields the following

$$\frac{\mu L_c U_i}{\left(1 - 0.351 \frac{e}{W_c}\right)^2} + \frac{\mu L_e V'_{N_c+1-i}}{\left(1 - 0.351 \frac{e}{W_{N_c+1-i}}\right)^2} = \frac{\mu L_c U_{i+1}}{\left(1 - 0.351 \frac{e}{W_c}\right)^2} + \frac{\mu L_e V_{i+1}}{\left(1 - 0.351 \frac{e}{W_{i+1}}\right)^2} \quad \text{(A4)}$$

In this equation as in the following, denominators are defined for ratios e/W_c and e/W_i ranging from zero to unity. Out of this range, the ratio should be replaced by its reciprocal value. Mass balances allow the velocities U_i with respect to V_i and V_{i+1}, and V'_{N_c+1-i} with respect to V_1 and V_{i+1} to be expressed as follows

$$U_i = \frac{W_i V_i - W_{i+1} V_{i+1}}{W_c} \quad \text{and} \quad V'_{N_c+1-i} = \frac{W_1 V_1 - W_{i+1} V_{i+1}}{W_{N_c+1-i}} \quad \text{(A5)}$$

Assuming a constant fluid viscosity in the plate and including the mass balances in the above equation yields

For $2 < i < N_c - 2$

$$-V_1 \frac{W_1 L_e}{W_{N_c+1-i}\left(1 - 0.351 \frac{e}{W_{N_c+1-i}}\right)^2} = V_i \left(\frac{W_i L_c}{W_c\left(1 - 0.351 \frac{e}{W_c}\right)^2}\right) + V_{i+2} \frac{W_{i+2} L_c}{W_c\left(1 - 0.351 \frac{e}{W_c}\right)^2} + V_{i+1}\left(-2 \frac{W_{i+1} L_c}{W_c\left(1 - 0.351 \frac{e}{W_c}\right)^2} - \frac{W_{i+1} L_e}{W_{N_c+1-i}\left(1 - 0.351 \frac{e}{W_{N_c+1-i}}\right)^2} - \frac{L_e}{\left(1 - 0.351 \frac{e}{W_{i+1}}\right)^2}\right) \quad \text{(A6)}$$

For $i = 1$

$$-V_1 \frac{W_1 L_e}{W_{N_c}\left(1 - 0.351 \frac{e}{W_{N_c}}\right)^2} - V_1\left(\frac{W_1 L_c}{W_c\left(1 - 0.351 \frac{e}{W_c}\right)^2}\right) = V_3 \frac{W_3 L_c}{W_c\left(1 - 0.351 \frac{e}{W_c}\right)^2} + V_2\left(-2 \frac{W_2 L_c}{W_c\left(1 - 0.351 \frac{e}{W_c}\right)^2} - \frac{W_2 L_e}{W_{N_c}\left(1 - 0.351 \frac{e}{W_{N_c}}\right)^2} - \frac{L_e}{\left(1 - 0.351 \frac{e}{W_2}\right)^2}\right) \quad \text{(A7)}$$

For $i = N_c - 1$

$$-V_1 \frac{W_1 L_e}{W_2\left(1 - 0.351 \frac{e}{W_2}\right)^2} = V_{N_c-1}\left(\frac{W_{N_c-1} L_c}{W_c\left(1 - 0.351 \frac{e}{W_c}\right)^2}\right) + V_{N_c}\left(-2 \frac{W_{N_c} L_c}{W_c\left(1 - 0.351 \frac{e}{W_c}\right)^2} - \frac{W_{N_c} L_e}{W_2\left(1 - 0.351 \frac{e}{W_2}\right)^2} - \frac{L_e}{\left(1 - 0.351 \frac{e}{W_{N_c}}\right)^2}\right) \quad \text{(A8)}$$

The following dimensionless parameters can now be introduced

$$V_i^+ = \frac{V_i}{V_1}, \quad W_i^+ = \frac{W_i}{e}, \; L^+ = \frac{L_c}{L_e} \quad \text{and} \quad W_c^+ = \frac{W_c}{e} \quad \text{(A9)}$$

The set of Eqs. A6 to A8 can be written as $AX = B$, where X is a vector composed of $N_c - 1$ dimensionless fluid velocities in inlet zones from V_2 to V_{N_c} and A a square matrix defined by

$$A(i,i) = -2\frac{W_{i+1}^+ L^+}{W_c^+\left(1-0.351\frac{1}{W_c^+}\right)^2} - \frac{W_{i+1}^+}{W_{N_c+1-i}^+\left(1-0.351\frac{1}{W_{N_c+1-i}^+}\right)^2} - \frac{1}{\left(1-0.351\frac{1}{W_{i+1}^+}\right)^2}$$

$$A(i,i-1) = \frac{W_i^+ L^+}{W_c^+\left(1-0.351\frac{1}{W_c^+}\right)^2}$$

$$A(i,i+1) = \frac{W_{i+2}^+ L^+}{W_c^{+\,+}\left(1-0.351\frac{1}{W_c^+}\right)^2} \tag{A10}$$

and B is defined by

$$B(1) = -\frac{W_1^+}{W_{N_c}^+\left(1-0.351\frac{1}{W_{N_c}^+}\right)^2} - \frac{W_1 L^+}{W_c^+\left(1-0.351\frac{1}{W_c^+}\right)^2}$$

$$B(i) = -\frac{W_1^+}{W_{N_c+1-i}^+\left(1-0.351\frac{1}{W_{N_c+1-i}^+}\right)^2} \text{ for } 2 \le i \le N_c - 2 \tag{A11}$$

Once the velocities have been calculated in the inlet zones, mass balances allow calculation of the velocities in the channels.

Appendix B: Condition on Chamber Geometry

The pressure drop relation for the approximate model (Eq. A3) results from the assumption that the boundaries of chamber zones are iso-pressure contours. As a result, pressure at the entrance to channel i and to inlet zone i are equal. Equal velocities in the channels imply equal pressure drops through the channels

$$\Delta P_{\text{channel } i} = \Delta P_{\text{channel } i+1} \quad \text{for} \quad 1 \le i \le N_c - 1 \tag{B1}$$

Using Eq. A3, the condition for a uniform velocity distribution implies

$$\Delta P_{\text{outlet zone } N_c+1-i} = \Delta P_{\text{inlet zone } i+1} \quad \text{for} \quad 1 \le i \le N_c - 1 \tag{B2}$$

For equal velocities U_c through channels, mass balances on the zones from i to N_c of inlet chambers and on the zones from i to N_c of the outlet chambers are, respectively

$$W_i V_i = (N_c + 1 - i) W_c U_c \qquad \text{and} \qquad W_i' V_i' = (N_c + 1 - i) W_c U_c \tag{B3}$$

For symmetric inlet and outlet chambers

$$W_i' = W_i \quad \text{which yields} \quad V_i' = V_i \quad \text{for} \quad 1 \le i \le N_c - 1 \tag{B4}$$

For the pressure drop relation A2, the equality condition can be rewritten as follows

$$\frac{N_c - i}{W_{i+1}^+\left(1-0.351\frac{1}{W_{i+1}^+}\right)^2} = \frac{i}{W_{N_c+1-i}^+\left(1-0.351\frac{1}{W_{N_c+1-i}^+}\right)^2} \tag{B5}$$

resulting in a direct relation between the width W_{i+1}^+ of inlet zone $i+1$ and the width $W_{N_c+1-i}^+$ of outlet zone $N_c + 1 - i$.

Manuscript received Feb. 5, 2001, and revision received July 11, 2001.